AMERICAN ACADEMY OF OPHTHALMOLOGY®

Increased Corneal Endothelial Cell Migration in Fuchs Endothelial Corneal Dystrophy

A Live Cell Imaging Study

Stephan Ong Tone, MDCM, PhD,[1,2,3,4,5] *Adam Wylegala, MD,*[1,2,3] *Myriam Böhm, MD,*[1,2,3] *Geetha Melangath, PhD,*[1,2,3] *Neha Deshpande, MSc,*[1,2,3] *Ula V. Jurkunas, MD*[1,2,3]

Purpose: To investigate if corneal endothelial cells (CECs) in Fuchs endothelial corneal dystrophy (FECD) have altered cellular migration compared with normal controls.

Design: Comparative analysis.

Materials: Descemet's membrane and CECs derived from patients with FECD undergoing endothelial keratoplasty or normal cadaveric donors.

Methods: Ex vivo specimens were used for live cell imaging and generation of immortalized cell lines. Live imaging was performed on FECD and normal CECs and on ex vivo specimens transfected with green fluorescent protein. Migration speeds were determined as a function of cellular density using automated cell tracking. Ex vivo specimens were classified as either FECD or normal low cell density (nonconfluent) or high cell density (confluent). Scratch assay was performed on CECs seeded at high confluence to determine migration speed. Genetic analysis from blood samples or CECs was performed to detect a CTG repeat expansion in the *TCF4* gene.

Main Outcome Measures: Mean cell migration speed.

Results: Fuchs endothelial corneal dystrophy CECs in low cell density areas displayed increased mean speed (0.391 ± 0.005 μm/minute vs. 0.364 ± 0.005 μm/minute; $P < 0.001$) and mean maximum speed (0.961 ± 0.010 μm/minute vs. 0.787 ± 0.011 μm/minute; $P < 0.001$) compared with normal CECs, and increased mean maximum speed (0.778 ± 0.014 μm/minute vs. 0.680 ± 0.011 μm/minute; $P < 0.001$) in high cell density areas ex vivo. Similarly, FECD CECs displayed increased mean speed compared with normal CECs (1.958 ± 0.020 μm/minute vs. 2.227 ± 0.021 μm/minute vs. 1.567 ± 0.019 μm/minute; $P < 0.001$) under nonconfluent conditions in vitro. Moreover, FECD CECs also displayed increased mean speed compared with normal CECs under high confluent conditions as detected by scratch assay ($37.2 \pm 1.1\%$ vs. $44.3 \pm 4.1\%$ vs. $70.7 \pm 5.2\%$; $P < 0.001$). Morphologic analysis showed that FECD CECs displayed an increased fibroblastic phenotype as detected by filamentous-actin labeling.

Conclusions: Fuchs endothelial corneal dystrophy CECs demonstrated increased migration speed compared with normal CECs. Further investigation into the mechanisms of heightened cell migration in FECD is needed and may provide insight into its pathogenesis, as well as having implications on descemetorhexis without endothelial keratoplasty. *Ophthalmology Science 2021;1:100006* © *2021 by the American Academy of Ophthalmology. This is an open access article under the CC BY-NC-ND license (http://creativecommons.org/licenses/by-nc-nd/4.0/).*

Supplemental material available at www.ophthalmologyscience.org/.

The corneal endothelium (CE) comprises a monolayer of hexagonal corneal endothelial cells (CECs) derived from neural crest cells that arise from the neuroectoderm[1] and rest on a specialized basement membrane called Descemet's membrane (DM). Corneal endothelial cells are postmitotic cells that are arrested in the G1 phase of the cell cycle and typically do not proliferate in vivo.[2] At birth, the human central cornea endothelial cell density (ECD) is approximately 4000 to 6000 cells/mm^2, and during the first 2 years of life, a decrease in ECD occurs likely because of an increase in corneal diameter with concurrent migration and spreading of CECs, rather than cell loss.[3–5] By 5 years of age, ECD is approximately 3500 cells/mm^2, which subsequently decreases throughout adulthood at an average rate of approximately 0.6% per year.[3,6] Although in many different cell types, cell division plays a major role in wound repair, cell division plays a limited role in the CE. Cell enlargement and cell migration largely are responsible for the wound-healing response in the CE.[2] However, as a consequence of excessive CEC loss, the wound-healing response can be overwhelmed and the CE no longer can maintain its barrier function and results in corneal edema.[2]

Fuchs endothelial corneal dystrophy (FECD) is the most common primary corneal endothelial dystrophy and the leading indication for corneal transplantation worldwide.[7] Fuchs endothelial corneal dystrophy typically manifests in

https://doi.org/10.1016/j.xops.2021.100006
ISSN 2666-9145/21

the fifth or sixth decades of life and has a greater incidence in women.[8–11] Fuchs endothelial corneal dystrophy is characterized by the progressive decline of CECs that leads to apoptosis, variation in size and shape, and the formation of abnormal extracellular matrix (ECM) excrescences called guttae.[8,12–15] Fuchs endothelial corneal dystrophy is a complex and genetically heterogeneous disease, with a strong genetic association to a trinucleotide CTG repeat expansion within the third intron of the transcription factor 4 (*TCF4*) gene.[16,17] Endothelial cell loss from FECD results in loss of barrier function and the inability of the CE to maintain fluid balance. No pharmacologic treatments are available for FECD, and corneal transplantation, typically endothelial keratoplasty, is the only treatment for FECD. More recently, a surgical technique termed *descemetorhexis without endothelial keratoplasty* (DWEK; also referred to as Descemet's stripping only) has been developed in which the central CE is removed without replacement with a corneal transplant.[18–22] Central corneal clearance after DWEK occurs as a result of the wound-healing response of the CE, where enlargement and migration of so-called normal-appearing CECs from the periphery occur. Despite the importance of CEC migration in DWEK, little is known about what regulates CEC migration in FECD. Few studies have investigated CEC migration behavior in normal donor CE,[23–25] and no studies have explored CEC migration directly in FECD ex vivo specimens. Therefore, to gain a better understanding of CEC migration in FECD, additional models are needed that use FECD specimens. These studies will provide information on CEC migration behavior and its potential impact on DWEK, as well as insight into FECD pathogenesis.

The purpose of this study was to investigate cellular migration speeds of human CECs in ex vivo FECD and normal specimens and in immortalized FECD and normal CECs derived from patient and cadaveric specimens, respectively (Fig 1A, B). To investigate cellular migration behavior of CECs, we established a novel live imaging model using lipid nanoparticle (LNP)-mediated green fluorescent protein (GFP) expression in CECs on ex vivo specimens from patients with FECD undergoing DMEK or normal cadaveric donor corneas. Genetic analysis from blood samples or CECs was performed to detect a CTG repeat expansion in the *TCF4* gene. Changes in cell morphologic features also were investigated.

Methods

Human Tissue

This study was conducted according to the tenets of the Declaration of Helsinki and was approved by the Massachusetts Eye and Ear Institutional Review Board. Written and informed consent was obtained from patients undergoing surgical treatment for FECD. After surgical removal, tissue was placed immediately in a storage medium (Optisol-GS; Bausch & Lomb) for 1 to 3 days before use. Normal donor corneas were purchased from Lions Vision Gift, CorneaGen, and Eversight and were kept in a storage medium for 5 to 13 days before use.

Cell Culture and Immortalization

Descemet's membrane and endothelium were collected from donor corneas (from a 67-year-old woman) and patients with FECD undergoing endothelial keratoplasty (n = 2, a 54-year-old woman and a 74-year-old woman). Specimens were incubated in complete Chen's medium (OptiMEM-I; Invitrogen) containing 8% fetal bovine serum (HyClone), 5 ng/ml epidermal growth factor (Millipore), 100 mg/ml bovine pituitary extract (Invitrogen), 200 mg/l calcium chloride (Sigma-Aldrich), 0.08% chondroitin sulfate (Sigma-Aldrich), 50 mg/ml gentamicin (Invitrogen), and 1:100 diluted antibiotic and antimycotic solution (Sigma-Aldrich) for 24 to 48 hours. Chen's medium was removed carefully with a 5-ml serologic pipette without disturbing the specimen. Specimens were incubated at 37° C, 5% CO_2, with 5 ml prewarmed 0.02% ethylenediaminetetraacetic acid (EDTA) solution (Sigma-Aldrich) for up to 45 minutes to disrupt cell-to-cell junctions and were examined periodically to visualize the disruption of cell-to-cell and cell-to-DM adhesions. Corneal endothelial cells were dissociated by gentle mechanical trituration (approximately 10 times) with a flame-polished pipette to disrupt cell junctions further. Corneal endothelial cells were centrifuged for 3 minutes at 3000 rpm at room temperature to pellet DM and cells. Corneal endothelial cells were resuspended in prewarmed Chen's media with gentle mechanical trituration and cells and DM were plated in a 24-well tissue culture plate precoated with undiluted FNC Coating (AthenaES). Corneal endothelial cells were incubated for approximately 48 hours at 37° C, 5% CO_2, before changing the media. Subculturing of CECs was performed using 0.05% trypsin (Invitrogen) for 5 minutes at 37° C, 5% CO_2. Primary CECs were immortalized using the simian virus-40 T-antigen cell immortalization kit (Alstem Cell Advancements). At passage 1, CECs were divided into 2 wells and infected with 2 µl/ml lentivirus (simian virus-40 T antigen) with 1 µl/ml TransPlus reagent (Alstem Cell Advancements). After 24 hours, viral supernatant was removed and CECs were grown in Chen's media for 72 hours. Transduced CECs underwent puromycin selection (2 µg/ml) until passage 5, after which they were grown in Chen's media without puromycin.

Live Imaging of Ex Vivo Specimens

Descemet's membrane and endothelium were collected from donor corneas (n = 3; age range, 60–68 years), and patients with FECD undergoing endothelial keratoplasty (n = 3; age range, 62–68 years). Normal and FECD specimens were incubated in Chen's medium for 24 to 48 hours in a 15-ml conical tube (Fischer Scientific) at 37° C, 5% CO_2, before transfection. For transfection with LNP GFP (Intellia Therapeutics, Cambridge, MA), LNP-mediated GFP (5–10 µg) was added to 500 µl of prewarmed Chen's media and mixed with 500 µl of 3% fetal bovine serum in prewarmed Chen's media and incubated at 37° C, 5% CO_2, for 5 minutes. Specimens then were transfected with 5 to 10 µg/ml LNP-GFP in 1 ml complete Chen's medium. After 24 hours, an additional 9 ml complete Chen's medium was added to the specimen and incubated for an additional 48 to 72 hours at 37° C, 5% CO_2. Descemet's membrane and endothelium were transferred gently using a 5-ml serologic pipette to a 12-well tissue culture plate precoated with undiluted FNC Coating. Excess media was removed gently using a 1-ml pipette tip, and the DM was positioned in the center of the well with the endothelium facing upward on top of the DM. A minimal touch technique was used whereby small drops of media were applied to the DM using a 1-ml pipette tip to open and unfold the DM using fluid to manipulate the positioning of the DM into a correct orientation. In certain cases, gentle manipulation of the DM at the periphery with

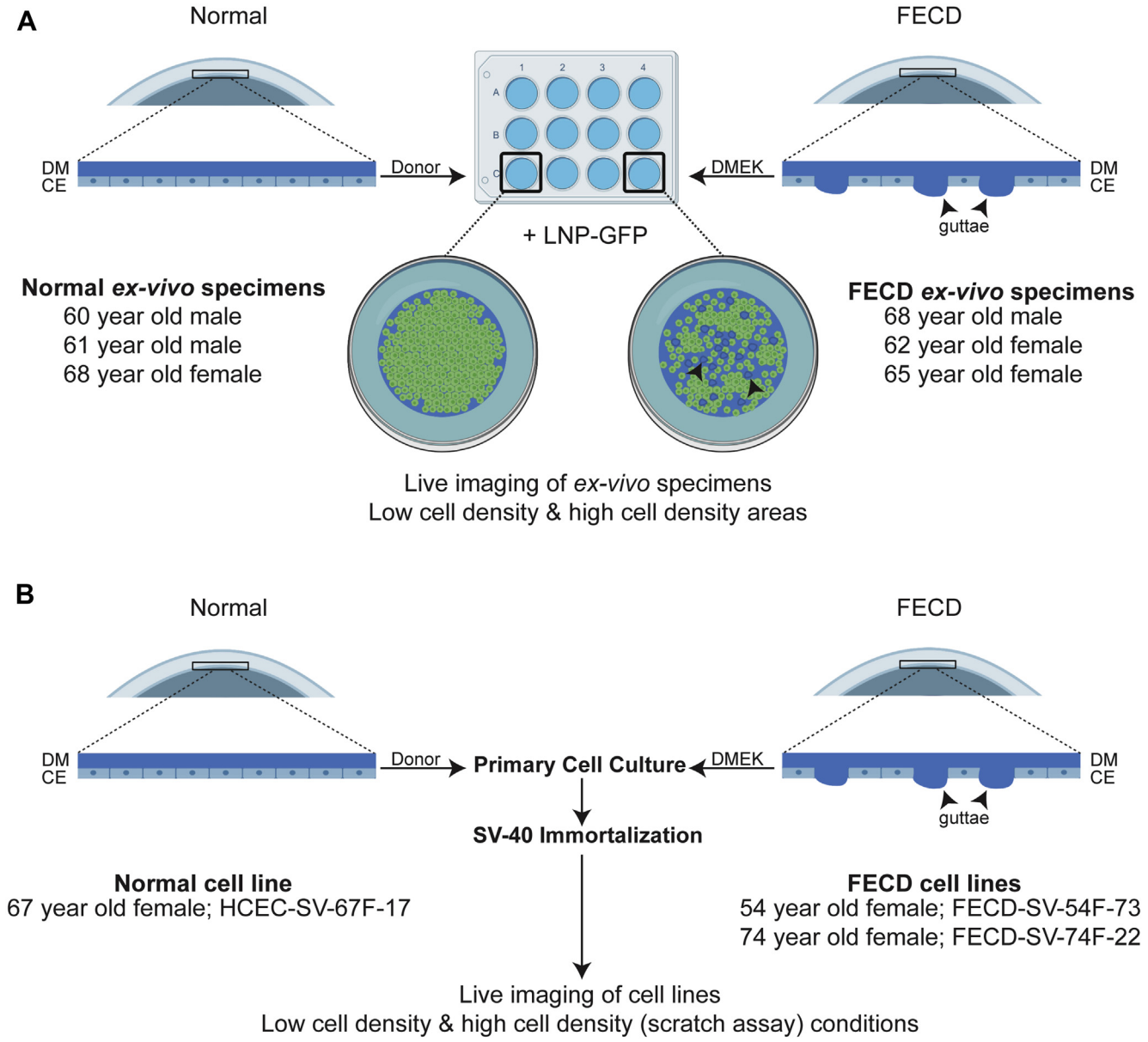

Figure 1. Experimental protocol of live cell imaging. Diagrams showing live cell imaging technique on (**A**) ex vivo specimens and (**B**) immortalized cell lines. Arrowheads indicate guttae. CE = corneal endothelium; DM = Descemet's membrane; DMEK = Descemet's membrane endothelial keratoplasty; FECD = Fuchs endothelial corneal dystrophy; HCEC = human corneal endothelial cell; LNP-GFP = lipid nanoparticle-green fluorescent protein; SV = simian virus.

fine-tipped forceps was needed to help position the DM. As soon as the specimen was unfolded and positioned with the correct orientation, a minimal amount of Chen's media was added to the well to cover the specimen completely. Live cell imaging was performed using the Leica DMi8 fluorescence inverted microscope (Leica Microsystems) at ×10 magnification with a motorized 3-plate stage (Leica) equipped with an all-in-one stage top incubator UNO-T-H-premixed (Okolab) with humidity and temperature (37° C) controllers and connected to a premixed 5% CO_2/95% air tank set at 15 psi gas flow. A 12-well tissue culture plate was placed on the Oko-H-301-K-frame (Okolab) with a 12-well plate holder and covered by an Oko-H-301-Koehler lid (Okolab). Images were acquired at 30-minute to 2-hour intervals over 15 to 20 hours. Four to 8 separate regions of interest were imaged per specimen, and 3 independent experiments were performed for analysis. Regions of interest were classified as either low cell density (nonconfluent), if cells were not in contact with other cells, or high cell density (confluent), if cells were in contact with adjacent cells, at the beginning of live imaging.

Scratch Assay and Nonconfluent Cell Migration Assay

Human CEC and FECD cell lines were grown to a confluent monolayer in a 12-well tissue culture plate precoated with undiluted FNC Coating, and a linear scratch was performed using a P200 pipette tip. For nonconfluent conditions, cells were plated at low cell density. Wells were washed with serum-free OptiMEM,

and live imaging was performed using a Leica DMi8 microscope at ×10 magnification acquiring images at 30-minute to 2-hour intervals over 16 to 18 hours. Three separate regions of interest were imaged per scratch or condition, and 3 independent experiments were performed for analysis. For scratch assay analysis, images were analyzed using Tscratch software as described previously.[26]

Cell Migration Analysis

Images acquired by live imaging were analyzed to determine cell migration speeds automatically (mean speed and mean maximum speed) using the Trackmate plugin in Fiji as described previously.[27] Briefly, image sequences were imported for analysis and the color mode was set to "default" with an autoscale and hyperstack view with ordering from X to T. We observed that CECs were relatively flat and traveled in the x-y plane, which made 2-dimensional analysis sufficient for the determination of migration speed. The Downsample LoG detector was used with an estimated blob diameter of 80 pixels and 0.25 threshold. Although most cells were identified automatically, a manual correction was performed to ensure that cells were identified accurately. A simple linear assignment problem (LAP) tracker was used with the following settings: gap closing distance of 2 frames, linking maximal distance of 120, and gap closing distance of 54. Tracks shorter than 2 frames also were excluded. Additional manual corrections were carried out in TrackScheme. The data were exported for subsequent statistical analysis.

Determination of *TCF4* Repeat Expansion

Genetic analysis with a short tandem repeat assay and triplet-repeat primed polymerase chain reaction was performed on genomic DNA extracted from blood samples and immortalized cells (Qiagen Blood & Tissue Kit) to identify expansion of the CTG repeat sequence in the *TCF4* gene as reported previously.[28]

Immunocytochemistry

Specimens and cell lines were fixed with 4% paraformaldehyde (Electron Microscopy Sciences) in ×1 phosphate-buffered saline (PBS; Boston Bioproducts) for 10 minutes at room temperature, followed by permeabilization with 0.2% Tx-100 (Sigma-Aldrich) in ×1 PBS for 5 minutes at room temperature or fixed with 100% acetone (Sigma-Aldrich) at −20° C for 10 minutes without subsequent permeabilization. Blocking was performed with 1% BSA in ×1 PBS for 1 hour at room temperature. Primary antibody was incubated overnight at 4° C (Invitrogen mouse anti-ZO-1, 1:100 dilution), and secondary antibody (Invitrogen anti-mouse-488, 1:100 dilution) and rhodamine-phalloidin (Cytoskeleton; 1:150 dilution) were incubated for 1 hour at room temperature. Specimens and cell lines were washed with ×1 PBS and incubated with DAPI (Thermo Fischer, 1:1000 dilution). Vectashield Antifade Mounting Medium (Vector Laboratories) and a coverglass were applied for imaging.

Cell Doubling Time

Human CEC and FECD cell lines were plated in duplicates in a 12-well tissue culture plate at a density of 50 000 cells per well. Media were changed on day 2. Cells were trypsinized, stained with trypan blue, and counted using a hemocytometer after 2, 3, and 4 days. Duplicate wells and 3 independent experiments were analyzed per cell line. Cell doubling time was calculated in the exponential phase of growth using the formula: $DT = T \ln 2 / \ln (Xe / Xb)$, in which DT is doubling time, T is incubation time, Xe is the cell number at end of incubation time, and Xb is the cell number at the beginning of incubation time.

Statistical Analysis

Statistical analysis was conducted using Statistica (Dell, Tulsa, OK) and Prism (GraphPad). The normality of the distribution of results was estimated using the Shapiro−Wilk test. Student's t test or the analysis of variance followed by the Bonferroni post hoc test was used to compare measured parameters. Values of $P < 0.05$ were considered to be statistically significant.

Results

No difference in mean age between normal donors and patients with FECD was found (63 ± 4 years vs. 65 ± 3 years; $P = 0.55$; Table 1). Normal or FECD ex vivo specimens were transfected transiently with LNP-GFP and were cultured for 3 days before live cell imaging to allow strong expression of GFP. Ex vivo specimens were positioned with the DM down in a culture well using a minimal touch technique that flattened most of the DM, but did result in some areas of DM folds (Fig 2A, top panels). Relaxing incisions to the DM were attempted but were aborted because of the excessive manipulation required, resulting in significant damage to the CECs (data not shown). Some areas of CEC loss were noted because of tissue manipulation for live imaging positioning (Fig 2A, top panels). High magnification live imaging showed GFP-expressing CECs in normal and FECD ex vivo specimens (Fig 2A, bottom panels). In FECD ex vivo specimens, CECs were visualized surrounding guttae (Fig 2A, bottom panels) and migrating adjacent to and on top of guttae (Video 1). The LNP-mediated GFP transfection of normal and FECD ex vivo specimens resulted in high transfection efficiency and GFP expression (Fig 2B).

To determine CEC migration speeds, multiple high cell density (confluent) areas and low cell density (nonconfluent) areas on normal and FECD ex vivo specimens were selected and imaged at 30-minute intervals over a 15- to 20-hour period (Fig 3A; Video 2). Normal nonconfluent CECs displayed increased mean speed compared with normal confluent CECs (0.364 ± 0.005 μm/minute vs. 0.280 ± 0.005 μm/minute; $P < 0.001$; Fig 3A, B). Similarly, FECD nonconfluent CECs displayed increased mean speed compared with FECD confluent CECs (0.391 ± 0.005 μm/minute vs. 0.277 ± 0.006 μm/minute; $P < 0.001$; Fig 3A, B). No difference in mean speed was found between normal and FECD confluent CECs (0.280 ± 0.005 μm/minute vs. 0.277 ± 0.006 μm/minute; $P = 0.67$; Fig 3A, B). However, FECD nonconfluent CECs displayed increased mean speed compared with normal nonconfluent CECs (0.391 ± 0.005 μm/minute vs. 0.364 ± 0.005 μm/minute; $P < 0.001$; Fig 3A, B). To determine if FECD CECs have an increased capacity for cellular migration compared with normal CECs, we calculated mean maximum speed. Normal nonconfluent CECs displayed increased mean maximum speed compared with normal confluent CECs (0.787 ± 0.011 μm/minute vs. 0.680 ± 0.011 μm/minute; $P < 0.001$; Fig 3B). Similarly, FECD nonconfluent CECs displayed increased

Table 1. Donor and Patient Characteristics

Specimen	Age (yrs)	Sex	Endothelial Cell Density (cells/mm^2)	Death to Preservation Time	Cause of Death	*TCF4* Repeat Status of Both Alleles	Use
Normal	67	F	2793	16 hrs 57 mins	Ovarian cancer	11/17	HCEC-SV-67F-17 cell line
Normal	60	M	2653	11 hrs 10 mins	Myocardial infarction	N/A	Live imaging
Normal	61	M	3021	6 hrs 30 mins	Cerebral vascular accident	N/A	Live imaging
Normal	68	F	2882	2 hrs 58 mins	Myocardial infarction	N/A	Live imaging
FECD	54	F	N/A	N/A	N/A	11/73	FECD-SV-54F-73 cell line
FECD	74	F	N/A	N/A	N/A	21/22	FECD-SV-74F-22 cell line
FECD	68	M	N/A	N/A	N/A	11/11	Live imaging
FECD	65	F	N/A	N/A	N/A	14/14	Live imaging
FECD	62	F	N/A	N/A	N/A	11/11	Live imaging

F = female; FECD = Fuchs endothelial corneal dystrophy; HCEC = human corneal endothelial cell; M = male; N/A = not applicable; *TCF4* = transcription factor 4; SV = simian virus.

mean maximum speed compared with FECD confluent CECs (0.961 ± 0.010 μm/minute vs. 0.778 ± 0.014 μm/minute; $P < 0.001$; Fig 3B). Fuchs endothelial corneal dystrophy confluent and nonconfluent CECs displayed increased mean maximum speed compared with normal confluent CECs (0.778 ± 0.014 μm/minute vs. 0.680 ± 0.011 μm/minute; $P < 0.001$) and nonconfluent CECs (0.961 ± 0.010 μm/minute vs. 0.787 ± 0.011 μm/minute; $P < 0.001$; Fig 3B). Genetic analysis was performed on genomic DNA from blood samples from the 3 patients with FECD that did not identify an expansion of the CTG repeat sequence in the *TCF4* gene (Table 1).

Because of limited FECD specimens available for ex vivo live imaging studies, we investigated whether the differences in CEC migrations speeds we observe in FECD ex vivo specimens also were recapitulated in immortalized human cell lines. We generated simian virus-40 immortalized human CEC lines derived from a normal cadaveric donor (HCEC-SV-67F-17) and 2 patients with FECD undergoing DMEK surgery (FECD-SV-54F-73 and FECD-SV-74F-22; Table 1). Genetic analysis was performed on genomic DNA from blood samples from the patients with FECD that identified a single allelic 73 repeat expansion of the CTG sequence in the *TCF4* gene in 1 of 2 patients with patients with FECD (FECD-SV-54F-73; Table 1). The other patient with FECD showed 22 repeats of the CTG sequence in the *TCF4* gene (FECD-SV-74F-22; Table 1), which was not considered expanded. Genetic analysis also was performed on genomic DNA from normal and FECD CECs that confirmed the CTG repeat expansion in FECD-SV-54F-73 and the lack of CTG repeat expansion in FECD-SV-74F-22 and HCEC-SV-67F-17 (Table 1). The CECs were plated under low cell density conditions (nonconfluent), and mean speed and mean maximum speed were measured (Fig 4A, B; Video 3). Both FECD-SV-54F-73 (1.958 ± 0.020 μm/minute vs. 1.567 ± 0.019 μm/minute; $P < 0.001$) and FECD-SV-74F-22 (2.227 ± 0.021 μm/minute vs. 1.567 ± 0.019 μm/minute; $P < 0.001$) displayed increased mean speed compared with HCEC-SV-67F-17 (Fig 4B). FECD-SV-74F-22 displayed increased mean speed compared with FECD-SV-54F-73 (2.227 ± 0.021 μm/minute vs. 1.958 ± 0.020 μm/minute; $P < 0.001$; Fig 4B). Both FECD-SV-54F-73 (5.806 ± 0.053 μm/minute vs. 4.910 ± 0.054 μm/minute; $P < 0.001$) and FECD-SV-74F-22 (5.618 ± 0.058 μm/minute vs. 4.910 ± 0.054 μm/minute; $P < 0.001$) displayed increased mean maximum speed compared with HCEC-SV-67F-17 (Fig 4B). No difference was found in mean maximum speed between FECD-SV-54F-73 and FECD-SV-74F-22 (5.806 ± 0.053 μm/minute vs. 5.618 ± 0.058 μm/minute; $P = 0.170$; Fig 4B).

To investigate further the difference in CEC migration speeds under confluent monolayer conditions, a scratch assay was performed, and wound-closure rates were calculated (Fig 5A, B; Video 4). Fuchs endothelial corneal dystrophy CECs (FECD-SV-54F-73 and FECD-SV-74F-22) displayed increased migration speed compared with normal CECs (HCEC-SV-67F-17) as detected by wound-closure rate between 10 to 16 hours after scratch initiation (Fig 5A, B). No differences in wound-closure rates were found between FECD-SV-54F-73 and FECD-SV-74F-22 at all time points (Fig 5A, B). To ensure that increased cell migration with FECD CECs detected with scratch assay was not secondary to increased cell proliferation rates, we determined cell doubling times of the CECs and found no differences (Supplemental Fig 1).

To investigate whether morphologic changes were present between normal and FECD CECs, normal and FECD ex vivo specimens were stained with rhodamine-phalloidin to label the filamentous-actin cytoskeleton. Normal ex vivo specimens displayed a compact and well-organized monolayer of hexagonal CECs with submembranous labeling of filamentous-actin (Fig 6A). In contrast, FECD ex vivo specimens displayed CECs with fibroblastic morphologic features, which included loss of hexagonality and elongated CECs (Fig 6A, white arrowhead), and CECs with filamentous-actin–rich lamellipodia at their leading edges (Fig 6A, white double arrowhead), suggesting that these CECs were spreading and initiating cellular migration. Furthermore, although normal and FECD CECs displayed cell–cell tight junctions as

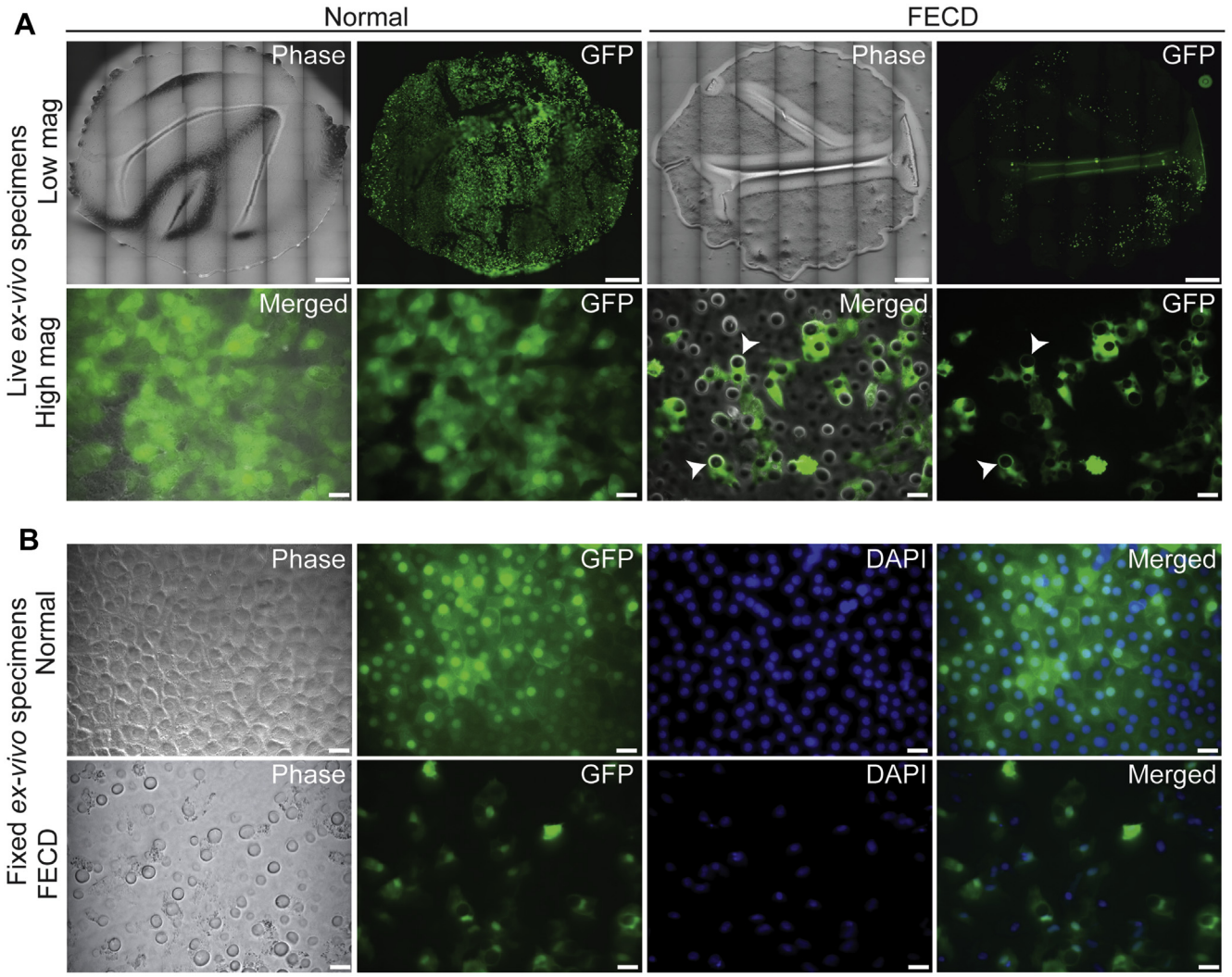

Figure 2. Live imaging of lipid nanoparticle (LNP)-mediated green fluorescent protein (GFP) expression in corneal endothelial cells (CECs) on normal and Fuchs endothelial corneal dystrophy (FECD) ex vivo specimens. **A**, Live imaging of normal and FECD ex vivo specimens. Low-magnification top panels show entire ex vivo specimens. Bottom panels show high magnification of GFP-expressing CECs on ex vivo specimens. Arrowhead indicates guttae. Scale bars = 1400 μm (top panels) and 25 μm (bottom panels). **B**, Paraformaldehyde-fixed ex vivo specimens showing expression of GFP in CECs of normal and FECD ex vivo specimens costained with DAPI to label DNA. Scale bars = 25 μm (bottom panels). Mag = magnification.

detected by zonular occludens 1 immunostaining, they also displayed more fibroblastic morphologic features as detected by filamentous-actin staining (Fig 6B).

Discussion

Herein, we describe a novel live imaging model using fluorescently labeled FECD ex vivo specimens to investigate CEC migration speeds at the individual cell resolution. We observed that FECD CECs in low cell density (nonconfluent) areas in ex vivo specimens displayed increased migration speeds as compared with normal controls. Furthermore, migration behavior occurred more as individual cell migration rather than monolayer spreading; no differences in mean migration speeds were observed in high cell density (confluent) areas, which we attributed to maintained cell-to-cell contact inhibition. However, we did observe that FECD CECs displayed increased maximum and mean migration speeds, suggesting that FECD CECs have an increased capacity for migration compared with normal controls. Consistent with our ex vivo data, FECD CECs derived from patients with FECD also displayed increased CEC migration speed compared with normal controls. We observed these differences in migration speed under both a low cell density (nonconfluent) condition with no cell-to-cell contact inhibition and under a high cell density (confluent) condition scratch assay that released cell-to-cell contact inhibition at the wound edge, resulting in directional migration to close the open area created by the scratch. We confirmed that differences in closure rates of the scratch wound were the result of increased cell migration rather than secondary to increased cell proliferation, because we found no differences in cell doubling times between the

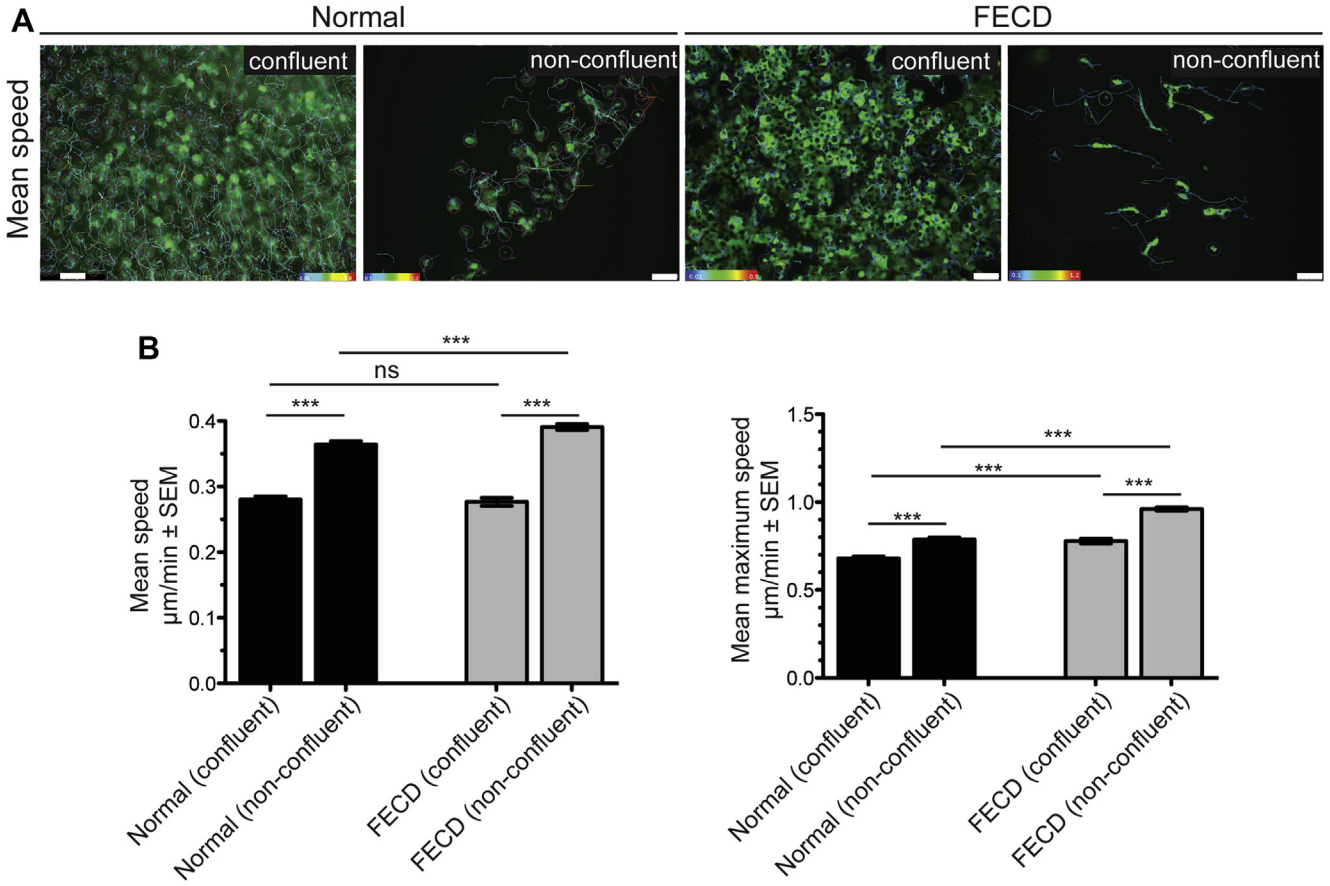

Figure 3. Increased cornea endothelial cell (CEC) migration speeds in Fuchs endothelial corneal dystrophy (FECD) ex vivo specimens compared with normal controls. **A**, Representative images of green fluorescent protein (GFP)-labeled CECs from high cell density (confluent) and low cell density (nonconfluent) areas on normal and FECD ex vivo specimens. Mean migration speed indicated by color maps. Scale bar = 100 µm. **B**, Bar graphs showing that nonconfluent normal and FECD CECs display increased mean speed compared with confluent CECs, nonconfluent FECD CECs display increased mean speed compared with normal CECs, nonconfluent normal and FECD CECs display increased mean maximum speed compared with confluent CECs, and nonconfluent and confluent FECD CECs display increased mean maximum speed compared with normal CECs. ***$P < 0.0001$, 1-way analysis of variance, post hoc Bonferroni test. ns = nonsignificant; SEM = standard error of the mean.

CECs. Morphologic analysis of FECD CECs revealed fibroblastic-type morphologic features. Overall, these findings suggest that FECD CECs undergo intrinsic promigratory changes that lead to increased cellular migration during dystrophic degeneration.

Fuchs endothelial corneal dystrophy pathogenesis has been attributed to a multitude of causes, including genetic, epigenetic, and exogenous factors ultimately leading to CEC apoptosis, senescence, and endothelial-to-mesenchymal transition (EMT).[15] As excessive cell loss occurs, the CE no longer can maintain its barrier function.[2,29] As CECs undergo apoptosis, this leads to areas devoid of CECs on the DM (Fig 6A), likely stimulating a wound-healing response of adjacent CECs through cell enlargement, monolayer spreading, and individual cell migration.[2] Endothelial-to-mesenchymal transition plays an important part in cellular migration, both during embryonic development and cellular invasion, and results in the loss of intercellular contacts, cellular polarity, and the acquisition of a fibroblastic phenotype.[30] In FECD, activation of EMT occurs with loss of normal CEC morphologic features, excessive production of ECM, as well as upregulation of EMT markers such as SNAI1, smooth muscle actin, ZEB1, fibronectin, N-cadherin, and transforming growth factor βI.[31–34] Although normal CECs are known to be arrested in the G0/G1 phase of the cell cycle, we recently showed that during stress, a paradoxical activation of the cell cycle and arrest in the G2/M phase occur that in turn lead to a profibrotic and EMT phenotype seen in FECD.[34] Herein, we further show that FECD cells exhibit a promigratory phenotype consistent with cellular adaptation to the stress response.

Although both cell proliferation and migration contribute to the formation of the CE from neural crest-derived mesenchymal cells during embryogenesis, the mature CE has limited capacity to proliferate, and the proliferation rate is not sufficient to replace entirely the loss of CECs.[2] After a small injury to the CE, enlargement of CECs occurs immediately adjacent to the wound, and membrane ruffling at the wound edge leads to wound closure.[35] This

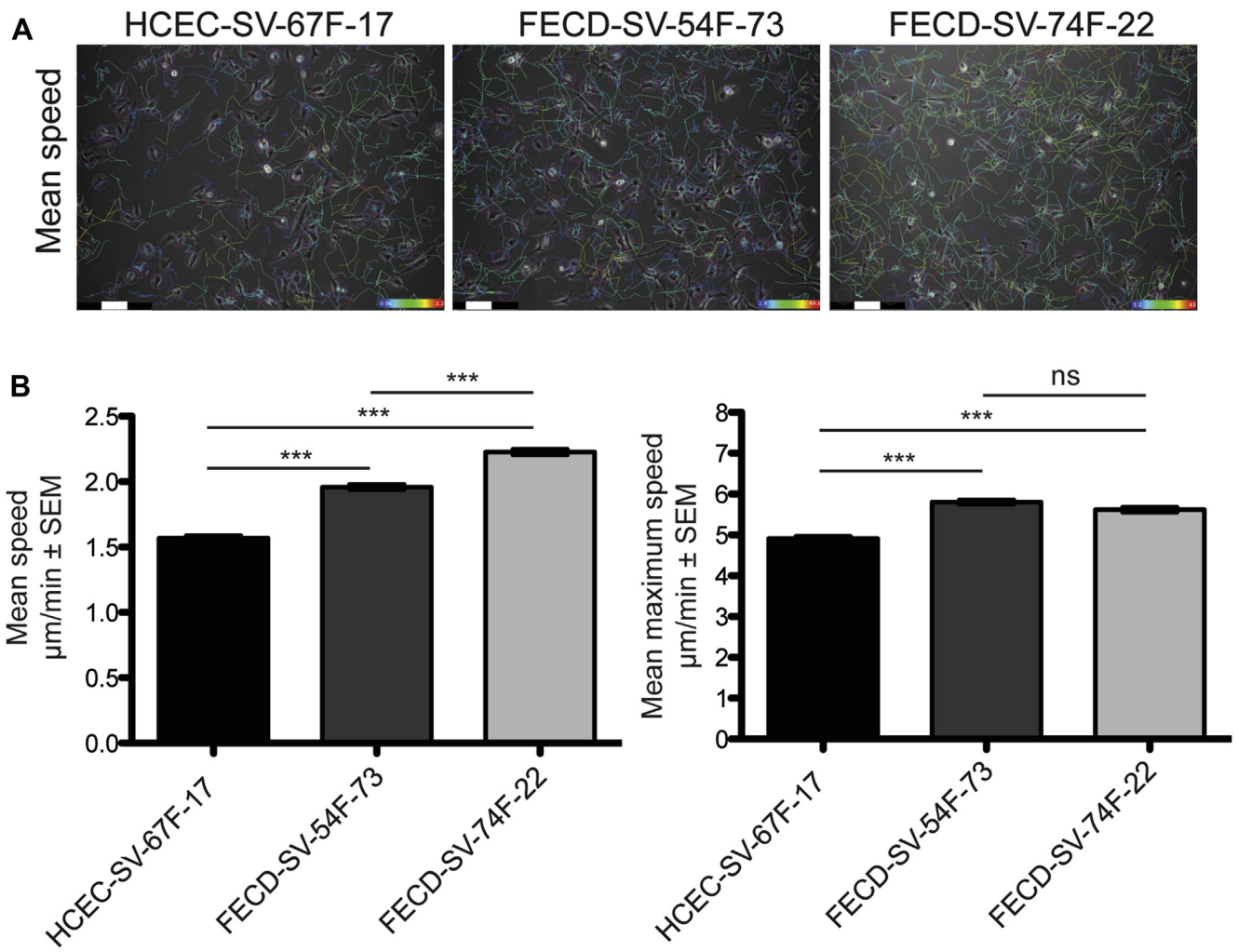

Figure 4. Increased corneal endothelial cell (CEC) migration speeds in nonconfluent conditions in Fuchs endothelial corneal dystrophy (FECD) compared with normal controls. **A**, Representative phase contrast images from nonconfluent normal and FECD CECs. Mean migration speed indicated by color maps. Scale bars = 100 µm. **B**, Bar graphs showing Fuchs endothelial corneal dystrophy CECs (FECD-SV-54F-73 and FECD-SV-74F-22) displaying increased mean speed and mean maximum speed compared with normal CECs (HCEC-SV-67F-17) and FECD-SV-74F-22 displaying increased mean speed compared with FECD-SV-54F-73. No difference in mean maximum speed between FECD-SV-74F-22 and FECD-SV-54F-73 was seen (n = 3). ***$P < 0.0001$, 1-way analysis of variance, post hoc Bonferroni test. ns = nonsignificant ($P = 0.17$); SEM = standard error of the mean.

observation is consistent with morphometric findings of human CECs in vivo, where age-related changes in cell size and shape are seen using specular microscopy.[2,36] However, after a larger wound, in addition to cell enlargement at the wound edge, a coordinated movement of adjacent surrounding cells that are contracted and pulled to close the wound occurs, a process termed *monolayer spreading*.[37–39] Additionally, individual cell migration contributes to this wound-healing response.[2,39] Thus, cell enlargement, cell spreading, and cell migration, in the absence of cell division, are the major mechanisms for wound repair in the adult human CE. Moreover, successful regeneration of the central CE after DWEK is dependent on the cellular migration of peripheral CECs, highlighting the importance of this wound-repair mechanism.

Despite the importance of CEC migration in FECD and DWEK, little is known about how CEC migration is affected in FECD. Although wound healing in the mature human CE occurs primarily through cell enlargement and migration, our study provides novel insight into this healing response during pathologic conditions. Some of the earlier studies focused on the ability of Rho-associated coiled-coil-containing protein kinase inhibition to promote normal CEC migration and proliferation.[40,41] Specifically, the major predictive factor for normal human CEC migration ex vivo was the presence of an intact DM during scratch wounds; intact DM was able to maintain the ECM microenvironment and facilitate CEC migration compared with a bare posterior stroma.[23] In our study, CEC migration behavior was observed on their native DM, where FECD CECs could migrate on their DM and interact with guttae. Given the importance of the ECM,[42–44] it is possible that altered ECM protein expression contributes to the increased CEC migration speed by providing a promigratory substrate for CECs to interact with. It was demonstrated previously that human CECs express the

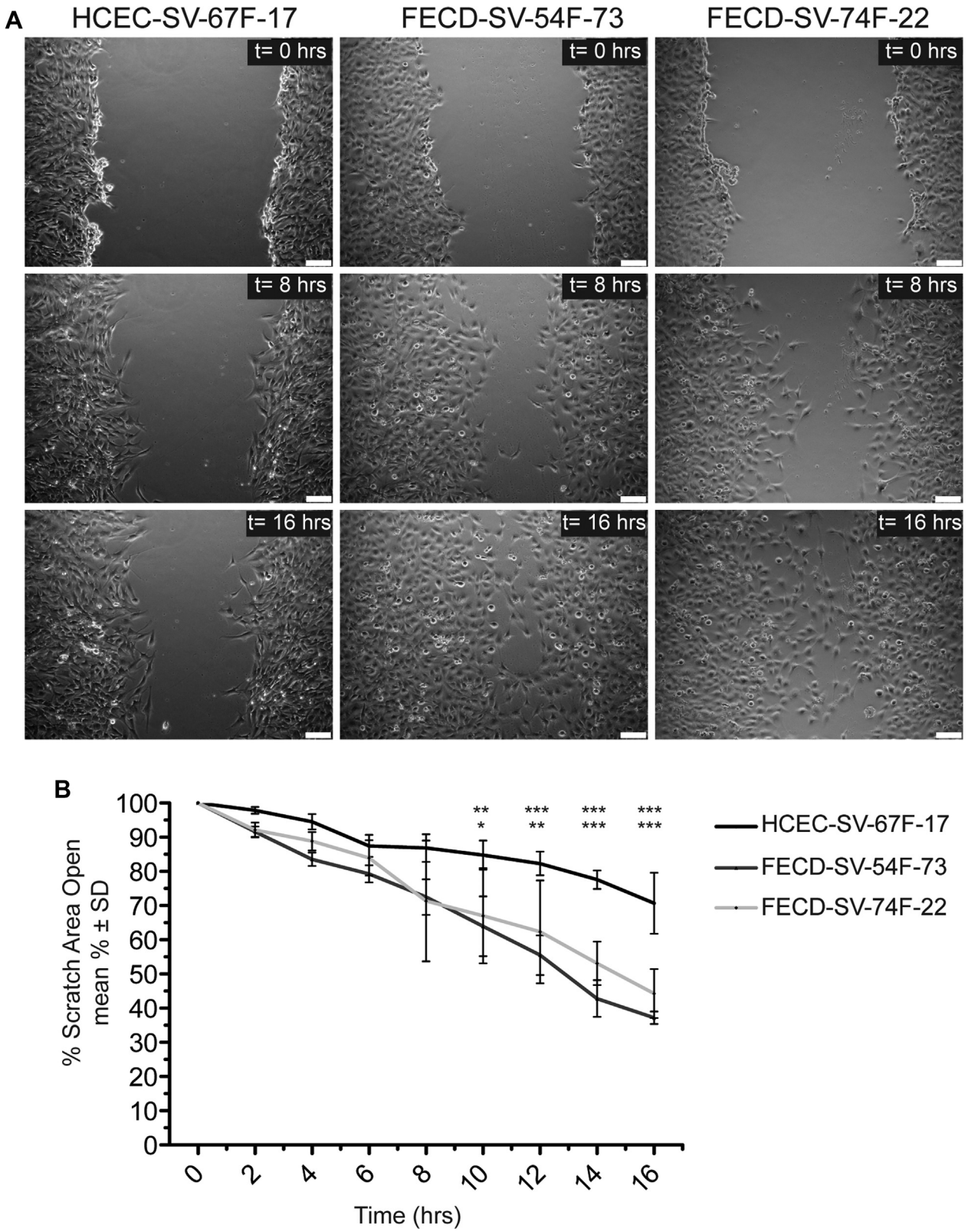

Figure 5. Increased corneal endothelial cell (CEC) migration speeds in confluent conditions in Fuchs endothelial corneal dystrophy (FECD) compared with normal controls as detected by scratch assay. **A**, Representative phase contrast images at 0 hours, 8 hours, and 16 hours after a scratch on a monolayer of CECs from normal (HCEC-SV-67F-17) and FECD (FECD-SV-54F-73 and FECD-SV-74—22) sources. Scale bars = 100 μm. **B**, Line graph showing FECD CECs (FECD-SV-54F-73 and FECD-SV-74F-22) displaying increased cell migration speed compared with normal CECs (HCEC-SV-67F-17) as detected by closure of scratch area (n = 3). $P < 0.0001$, 2-way analysis of variance post hoc Bonferroni test. *$P < 0.05$. **$P < 0.01$. ***$P < 0.001$. ns = nonsignificant; SD = standard deviation.

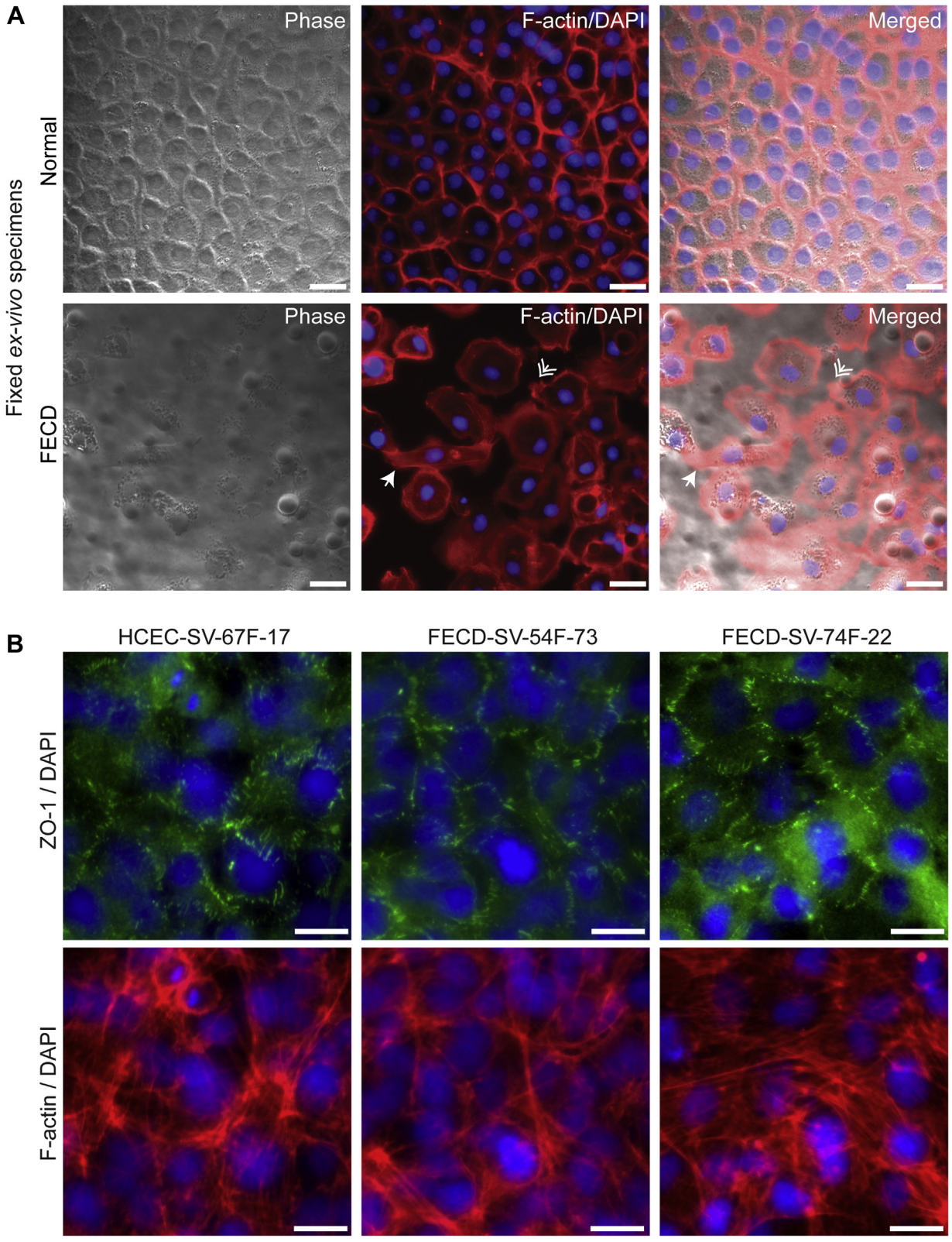

Figure 6. Fuchs endothelial corneal dystrophy (FECD) corneal endothelial cells (CECs) display fibroblastic morphologic features. **A**, Phase contrast, filamentous-actin (f-actin; red), and DAPI-labeled (blue) normal and FECD ex vivo specimens. White arrowhead indicates fibroblastic CECs, and white double arrowhead indicates lamellipodia at CEC border. Scale bars = 25 μm. **B**, Normal (HCEC-SV-67F-17) and FECD (FECD-SV-54F-73 and FECD-SV-74F-22) CECs immunostained for zonular occludens-1 (ZO-1; green), f-actin (red), and DAPI (blue). Scale bars = 10 μm.

laminin receptor α3β1 integrin and that its ECM ligand laminin-5 promotes adhesion, proliferation, and migration of CECs.[44] In FECD, alterations in expression of ECM proteins such as fibronectin; integrin β5; collagen types III and XVI; agrin; transforming growth factor βI; and clusterin have been reported.[45,46] Furthermore, differences in migration speed have been reported when normal CECs are seeded on normal DM or FECD DM, highlighting the capacity of the ECM to affect CEC behavior.[33] Our observation that FECD CECs display increased migration speeds compared with normal CECs on the same substrate supports the hypothesis that FECD CECs have intrinsic promigratory changes, in addition to potential ECM changes, that contribute to its increased migration phenotype.

Although this study provides novel insight into the behavior of CECs migrating on their native DM in normal and FECD ex vivo specimens, these observations must be taken in the context that ex vivo culture conditions may be different from in vivo conditions. Furthermore, although immortalized cell lines provided us with the opportunity to perform numerous experiments to explore cell migration behavior, morphologic characteristics, and gene expression in FECD, it is plausible that these findings do not recapitulate primary cells or in vivo cells entirely because differences in gene expression have been reported previously.[47]

This study demonstrated that FECD CECs display increased cell migration speed, which may impact cellular migration during DWEK. Although certain factors were identified previously to help predict corneal clearance after DWEK, including surgical technique of stripping DM,[18,48] descemetorhexis size,[48,49] and peripheral ECD,[49] additional factors including age, sex, and genetic factors remain to be investigated fully. Identifying these preoperative factors is essential in selecting which patients are most likely to respond to DWEK. For example, understanding how the CTG repeat expansion in *TCF4*, the most common genetic mutation in FECDs, affects CEC migration may provide guidance on patient selection for DWEK. Currently, several mechanisms have been proposed to explain the link between the CTG repeat expansion in *TCF4* and FECD, including *TCF4* dysregulation, toxic gain of function, toxic repeat-associated non-AUG translation, and somatic instability.[17] Furthermore, *TCF4* has been reported as an important regulator of EMT, in which increased *TCF4* expression can drive EMT.[50] However, further investigation into how the genetics of FECD contribute to CEC migration is needed, which may provide further insight into FECD pathogenesis and may predict a patient's response to DWEK.

Acknowledgments

The authors thank Celina Wu for assistance with the illustrations, which were created with BioRender.com.

Footnotes and Disclosures

Originally received: November 11, 2020.
Final revision: February 9, 2021.
Accepted: March 3, 2021.
Available online: March 9, 2021. Manuscript no. D-20-00020.

[1] Cornea Center of Excellence, Schepens Eye Research Institute, Harvard Medical School, Boston, Massachusetts.

[2] Massachusetts Eye and Ear Infirmary, Harvard Medical School, Boston, Massachusetts.

[3] Department of Ophthalmology, Harvard Medical School, Boston, Massachusetts.

[4] Sunnybrook Health Sciences Centre, Sunnybrook Research Institute, Toronto, Canada.

[5] Department of Ophthalmology, University of Toronto, Toronto, Canada.

Presented at: American Academy of Ophthalmology Annual Meeting, October 2019, San Francisco, California.

Disclosure(s):
All authors have completed and submitted the ICMJE disclosures form.

The author(s) have made the following disclosure(s): A.W.: Consultant — Zeiss Meditec; Financial support — Optopol Technology; Lecturer - MDT

U.V.J.: Consultant — Senju, Chesi; Financial support — Kowa, Santen Pharmaceuticals, Intellia

Supported by the National Eye Institute, National Institutes of Health, Bethesda, Maryland (grant no.: R01 EY020581 [U.V.J.]); the Eversight Foundation (U.V.J.); Shire Research Scholarship (S.O.T.); the European Society of Cataract and Refractive Surgery (Peter Barry Fellowship [M.B.]); and the Kosciuszko Foundation (A.W.). The sponsor or funding organization had no role in the design or conduct of this research.

HUMAN SUBJECTS: Human subjects were included in this study. The human ethics committees at Massachusetts Eye and Ear approved the study. All research adhered to the tenets of the Declaration of Helsinki. All participants provided informed consent.

No animal subjects were included in this study.

Author Contributions:

Conception and design: Ong Tone, Wylegala, Böhm, Melangath, Deshpande, Jurkunas

Analysis and interpretation: Ong Tone, Wylegala, Böhm, Melangath, Deshpande, Jurkunas

Data collection: Ong Tone, Wylegala, Böhm, Melangath, Deshpande, Jurkunas

Obtained funding: Jurkunas; Study was performed as part of regular employment duties at Massachusetts Eye and Ear. No additional funding was provided.

Overall responsibility: Ong Tone, Wylegala, Böhm, Melangath, Deshpande, Jurkunas

Abbreviations and Acronyms:
CE = corneal endothelium; **CEC** = corneal endothelial cell; **DM** = Descemet's membrane; **DMEK** = Descemet's membrane endothelial keratoplasty; **DWEK** = descemetorhexis without endothelial keratoplasty; **ECD** = endothelial cell density; **ECM** = extracellular matrix; **EMT** = endothelial-to-mesenchymal transition; **FECD** = Fuchs endothelial corneal dystrophy; **GFP** = green fluorescent protein; **LNP** = lipid nanoparticle; **PBS** = phosphate-buffered saline; **TCF4** = transcription factor 4.

Keywords:
Cell migration, Corneal endothelium, Descemetorhexis without endothelial keratoplasty, Descemet's stripping only, Fuchs endothelial corneal dystrophy.

Correspondence:
Ula V. Jurkunas, MD, Cornea Center of Excellence, Department of Ophthalmology, Harvard Medical School, Massachusetts Eye and Ear Infirmary, Schepens Eye Research Institute, 20 Staniford Street, Boston, MA 02114. E-mail: ula_jurkunas@meei.harvard.edu; and Stephan Ong Tone, MDCM, PhD, Sunnybrook Health Sciences Centre and Sunnybrook Research Institute, Department of Ophthalmology and Vision Sciences, University of Toronto, 2075 Bayview Avenue, M Wing, 1st Floor, Toronto, Ontario M4N 3M5, Canada. E-mail: stephan.ongtone@sunnybrook.ca.

References

1. Katikireddy KR, Schmedt T, Price MO, et al. Existence of neural crest−derived progenitor cells in normal and Fuchs endothelial dystrophy corneal endothelium. *Am J Pathol*. 2016;186(10):2736−2750.
2. Joyce N. Proliferative capacity of the corneal endothelium. *Prog Retin Eye Res*. 2003;22(3):359−389.
3. Elbaz U, Mireskandari K, Tehrani N, et al. Corneal endothelial cell density in children: normative data from birth to 5 years old. *Am J Ophthalmol*. 2017;173:134−138.
4. Speedwell L, Novakovic P, Sherrard ES, Taylor DSI. The infant corneal endothelium. *Arch Ophthalmol*. 1988;106(6):771−775.
5. Williams KK, Noe RL, Grossniklaus HE, et al. Correlation of histologic corneal endothelial-cell counts with specular microscopic cell-density. *Arch Ophthalmol*. 1992;110(8):1146−1149.
6. Bourne WM, Nelson LR, Hodge DO. Central corneal endothelial cell changes over a ten-year period. *Invest Ophthalmol Vis Sci*. 1997;38(3):779−782.
7. Gain P, Jullienne R, He Z, et al. Global survey of corneal transplantation and eye banking. *JAMA Ophthalmol*. 2016;134(2):167−173.
8. Krachmer JH. Corneal endothelial dystrophy. *Arch Ophthalmol*. 1978;96(11):2036−2039.
9. Afshari NA. Clinical study of Fuchs corneal endothelial dystrophy leading to penetrating keratoplasty. *Arch Ophthalmol*. 2006;124(6):777−780.
10. Louttit MD, Kopplin LJ, Igo RP, et al. A multicenter study to map genes for Fuchs endothelial corneal dystrophy: baseline characteristics and heritability. *Cornea*. 2012;31(1):26−35.
11. Minear MA, Li YJ, Rimmler J, et al. Genetic screen of African Americans with Fuchs endothelial corneal dystrophy. *Mol Vis*. 2013;19:2508−2516.
12. Jun A, Vedana G, Villarreal Jr G. Fuchs endothelial corneal dystrophy: current perspectives. *Clin Ophthalmol*. 2016;10:321.
13. Jun AS. One hundred years of Fuchs' dystrophy. *Ophthalmology*. 2010;117(5):859−860.e14.
14. Vogt A. Weitere Ergebnisse der Spaltlampenmikroskopie des vordern Bulbusabschnittes. *Arch Ophthalmol*. 1921:63−113.
15. Ong Tone S, Kocaba V, Böhm M, et al. Fuchs endothelial corneal dystrophy: the vicious cycle of Fuchs pathogenesis. *Prog Retin Eye Res*. 2021;80:100863.
16. Lewin A, Wieben ED, Aleff RA, et al. A common trinucleotide repeat expansion within the transcription factor 4 (TCF4, E2-2) gene predicts Fuchs corneal dystrophy. *PLoS One*. 2012;7(11):e49083.
17. Fautsch MP, Wieben ED, Baratz KH, et al. TCF4-mediated Fuchs endothelial corneal dystrophy: insights into a common trinucleotide repeat-associated disease. *Prog Retin Eye Res*. 2020:100883.
18. Arbelaez JG, Price MO, Price FW. Long-term follow-up and complications of stripping Descemet membrane without placement of graft in eyes with Fuchs endothelial dystrophy. *Cornea*. 2014;33(12):1295−1299.
19. Shah RD, Randleman JB, Grossniklaus HE. Spontaneous corneal clearing after Descemet's stripping without endothelial replacement. *Ophthalmology*. 2012;119(2):256−260.
20. Borkar DS, Veldman P, Colby KA. Treatment of Fuchs endothelial dystrophy by Descemet stripping without endothelial keratoplasty. *Cornea*. 2016;35(10):1267−1273.
21. Koenig SB. Planned descemetorhexis without endothelial keratoplasty in eyes with Fuchs corneal endothelial dystrophy. *Cornea*. 2015;34(9):1149−1151.
22. Koenig SB. Long-term corneal clarity after spontaneous repair of an iatrogenic descemetorhexis in a patient with Fuchs dystrophy. *Cornea*. 2013;32(6):886−888.
23. Soh YQ, Peh G, George BL, et al. Predicative factors for corneal endothelial cell migration. *Invest Opthalmol Vis Sci*. 2016;57(2):338−348.
24. Miron A, Spinozzi D, Bruinsma M, et al. Asymmetrical endothelial cell migration from in vitro quarter-Descemet membrane endothelial keratoplasty grafts. *Acta Ophthalmol*. 2018;96(8):828−833.
25. Deng SX, Miron A, Spinozzi D, et al. In vitro endothelial cell migration from limbal edge-modified quarter-DMEK grafts. *Plos One*. 2019;14(11):e0225462.
26. Gebäck T, Schulz MMP, Koumoutsakos P, Detmar M. TScratch: a novel and simple software tool for automated analysis of monolayer wound healing assays. *Biotechniques*. 2009;46(4):265−274.
27. Tinevez J-Y, Perry N, Schindelin J, et al. TrackMate: an open and extensible platform for single-particle tracking. *Methods*. 2017;115:80−90.
28. Vasanth S, Eghrari AO, Gapsis BC, et al. Expansion of CTG18.1 trinucleotide repeat in TCF4 is a potent driver of Fuchs' corneal dystrophy. *Invest Opthalmol Vis Sci*. 2015;56(8):4531−4536.
29. Crawford KM, Ernst SA, Meyer RF, MacCallum DK. NaK-ATPase pump sites in cultured bovine corneal endothelium of varying cell density at confluence. *Invest Opthalmol Vis Sci*. 1995;36(7):1317−1326.
30. Campbell K, Casanova J. A common framework for EMT and collective cell migration. *Development*. 2016;143(23):4291−4300.
31. Katikireddy KR, White TL, Miyajima T, et al. NQ01 downregulation potentiates menadione-induced endothelial-mesenchymal transition during rosette formation in Fuchs endothelial corneal dystrophy. *Free Rad Biol Med*. 2018;116:19−30.
32. Okumura N, Minamiyama R, Ho LTY, et al. Involvement of ZEB1 and Snai11 in excessive production of extracellular matrix in Fuchs endothelial corneal dystrophy. *Lab Invest*. 2015;95(11):1291−1304.

33. Kocaba V, Katikireddy KR, Gipson I, et al. Association of the gutta-induced microenvironment with corneal endothelial cell behavior and demise in Fuchs endothelial corneal dystrophy. *JAMA Ophthalmol*. 2018;136(8):886.
34. White TL, Deshpande N, Kumar V, et al. Cell cycle re-entry and arrest in G2/M phase induces senescence and fibrosis in Fuchs endothelial corneal dystrophy. *Free Rad Biol Med*. 2021;164:34−43.
35. Sherrard ES. The corneal endothelium in vivo: its response to mild trauma. *Exp Eye Res*. 1976;22(4):347−357.
36. Laing RA, Sandstrom MM, Berrospi AR, Leibowitz HM. Changes in the corneal endothelium as a function of age. *Exp Eye Res*. 1976;22(6):587−594.
37. Honda H, Ogita Y, Higuchi S, Kani K. Cell movements in a living mammalian tissue: long-term observation of individual cells in wounded corneal endothelia of cats. *J Morphol*. 1982;174(1):25−39.
38. Kaufman HE, Katz JI. Pathology of the corneal endothelium. *Invest Opthalmol Vis Sci*. 1977;16(4):265−268.
39. Joyce NC, Meklir B, Neufeld AH. In vitro pharmacologic separation of corneal endothelial migration and spreading responses. *Invest Opthalmol Vis Sci*. 1990;31(9):1816−1826.
40. Lee JG, Kay EP. FGF-2-induced wound healing in corneal endothelial cells requires Cdc42 activation and Rho inactivation through the phosphatidylinositol 3-kinase pathway. *Invest Opthalmol Vis Sci*. 2006;47(4):1376−1386.
41. Meekins LC, Rosado-Adames N, Maddala R, et al. Corneal endothelial cell migration and proliferation enhanced by Rho kinase (ROCK) inhibitors in in vitro and in vivo models. *Invest Opthalmol Vis Sci*. 2016;57(15):6731−6738.
42. Koo S, Muhammad R, Peh GSL, et al. Micro- and nano-topography with extracellular matrix coating modulate human corneal endothelial cell behavior. *Acta Biomaterialia*. 2014;10(5):1975−1984.
43. Okumura N, Kakutani K, Numata R, et al. Laminin-511 and -521 enable efficient in vitro expansion of human corneal endothelial cells. *Invest Opthalmol Vis Sci*. 2015;56(5):2933−2942.
44. Yamaguchi M, Ebihara N, Shima N, et al. Adhesion, migration, and proliferation of cultured human corneal endothelial cells by laminin-5. *Invest Opthalmol Vis Sci*. 2011;52(2):679−684.
45. Goyer B, Thériault M, Gendron SP, et al. Extracellular matrix and integrin expression profiles in Fuchs endothelial corneal dystrophy cells and tissue model. *Tissue Eng Part A*. 2018;24(7−8):607−615.
46. Weller JM, Zenkel M, Schlötzer-Schrehardt U, et al. Extracellular matrix alterations in late-onset Fuchs' corneal dystrophy. *Invest Opthalmol Vis Sci*. 2014;55(6):3700−3708.
47. Frausto RF, Le DJ, Aldave AJ. Transcriptomic analysis of cultured corneal endothelial cells as a validation for their use in cell replacement therapy. *Cell Transplant*. 2016;25(6):1159−1176.
48. Davies E, Jurkunas U, Pineda R. Predictive factors for corneal clearance after descemetorhexis without endothelial keratoplasty. *Cornea*. 2018;37(2):137−140.
49. Moloney G, Petsoglou C, Ball M, et al. Descemetorhexis without grafting for Fuchs endothelial dystrophy—supplementation with topical ripasudil. *Cornea*. 2017;36(6):642−648.
50. Sobrado VR, Moreno-Bueno G, Cubillo E, et al. The class I bHLH factors E2-2A and E2-2B regulate EMT. *J Cell Sci*. 2009;122(7):1014−1024.